

Computer Simulation of Dislocation Loops in Cu and Fe

E. Kuramoto and T. Tsutsumi

Research Institute for Applied Mechanics, Kyushu University

Interstitial type dislocation loops were formed in the model lattices of Cu and Fe to investigate the atomic structures as a function of loop size, especially to clarify the transition from clusters of self-interstitial atoms to dislocation loops. It was found that the localized strain of a crowdion on the $\langle 110 \rangle$ atomic row in Cu is not maintained in the clusters of crowdions (more than about 10 crowdions), but is split into two parts along the $\langle 110 \rangle$ atomic row on which the original crowdion is placed. The same tendency was observed in the clusters of $\langle 111 \rangle$ crowdions in Fe. These suggest that clusters of crowdions are changing into dislocation loops as increasing number of component interstitial atoms.

1. INTRODUCTION

In the research of radiation damage in materials used in high temperature and high dose irradiation condition behaviours of small interstitial clusters have been recognized very important because they definitely affect the evolution of total damage structure through bias effects, especially production bias (1). In the case of irradiation where cascade formation of defects occurs it is known that spontaneous formation of interstitial clusters, namely small dislocation loops takes place in the outer region of cascades and these loops are mobile and easily move on the straight way to sinks, such as dislocations during irradiation (2). As increasing the number of self-interstitial atoms which construct the interstitial clusters, these clusters might be changed into dislocation loops and dislocation lines, but detailed features on this point have not been investigated. In this paper the atomic structure of the interstitial type dislocation loops will be investigated by computer simulation using N-body type interatomic potentials as a function of loop size in Cu (fcc case) and Fe (bcc case). Possibility of movement of these small dislocation loops under the external stress will also

be studied.

2. METHOD OF CALCULATION

Model crystals of Cu and Fe which have size of about $60b \times 60b \times 60b$ (b : Strength of Burgers Vector) were used, where interstitial loops are placed at the central part on $\{111\}$ plane in Cu and on $\{110\}$ plane in Fe as shown in Fig. 1. The interatomic potentials used are N-body type potentials developed by Ackland et al. for Cu (3) and by Finnis-Sinclair for Fe (4). The whole lattice with an interstitial cluster was completely relaxed statically except the boundary region and the final atomic configuration and the total energy were obtained.

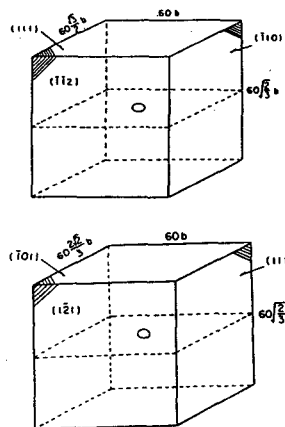


Fig. 1 Model lattices for Cu (upper) and for Fe (below)

3. RESULTS AND DISCUSSION

3.1 Dislocation Loops in Cu

Three kinds of the small interstitial loops, namely, i) $a/2\langle 110 \rangle\{111\}$ perfect loop, ii) $a\langle 100 \rangle\{111\}$ faulted loop and iii) $a/3\langle 111 \rangle\{111\}$ faulted loop were constructed in the model lattice. One example of the loop structure in Cu is shown in Fig.2, where $a/2\langle 110 \rangle\{111\}$ perfect loop consisting of 19 self interstitial atoms ($\langle 110 \rangle$ crowdions) is drawn through the top view and the side view. In this case no stacking fault is seen, but in other two cases, i.e., $a\langle 100 \rangle\{111\}$ faulted loop and $a/3\langle 111 \rangle\{111\}$ faulted loop, stacking faults are observed. The formation energy and the binding energy per one interstitial atom were calculated for each type of the dislocation loop as a function of the number of the component interstitial atoms and the binding energy for $a/2\langle 110 \rangle\{111\}$ perfect loop is shown in Fig. 3. The comparison between $a/2\langle 110 \rangle\{111\}$ perfect loop and $a\langle 100 \rangle\{111\}$ faulted loop is shown in Fig. 4, which shows that the faulted loop is more stable than the perfect loop in the region of small number of interstitial atoms ($n < 100$). The formation energy decreased in the order of $a/2\langle 110 \rangle\{111\}$ perfect loop, $a/3\langle 111 \rangle\{111\}$ faulted loop and $a\langle 100 \rangle\{111\}$ faulted loop. The first one and the last one consist of $\langle 111 \rangle$ crowdions and $\langle 100 \rangle$ dumbbells, respectively, but in $a/3\langle 111 \rangle\{111\}$ faulted loop $\langle 111 \rangle$ interstitial atoms were inclined to $\langle 112 \rangle$ direction during relaxation.

For the case of $a/2\langle 110 \rangle\{111\}$ perfect loop more detailed investigation of the loop structure was made, namely, the strain distribution (change of the interatomic distance) on the atomic row on which each component crowdion is located was obtained as a function of loop size and a position of the atomic row of the crowdion and the result is shown in Fig. 5. It is found that in small interstitial clusters the strain is localized as in the case of single crowdion, but in the larger clusters ($n > 10$) it is split into two parts. This means that the interstitial clusters tend to have the character of a dislocation. To confirm this the strain

distribution on the atomic row on the peripheral position of the loop was also obtained, which also shows the split strain distribution as shown in Fig. 6 for the interstitial cluster of 91 crowdions. But, this feature depends on the peripheral position, namely, the strain distribution is split on $\{111\}$ planes, but is not split on $\{100\}$ planes. The loop has a hexagonal shape and $4/6$ of the $\langle 111 \rangle$ atomic rows on the peripheral position lies on $\{111\}$ plane and $2/6$ lies on the $\{100\}$ plane.

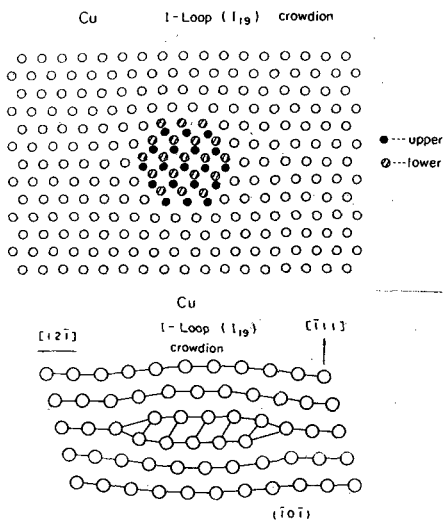


Fig. 2 Atomic structure I-loop (I_{19}) in Cu

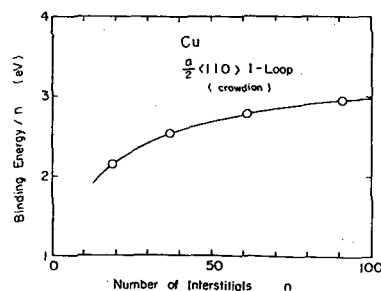


Fig. 3 Binding energy as a function of loop size in Cu

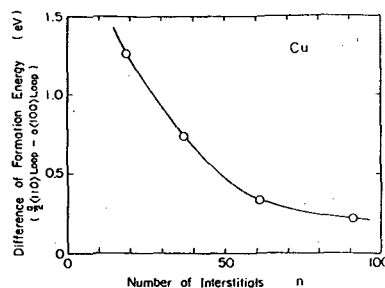


Fig. 4 Formation energies of perfect and faulted loops

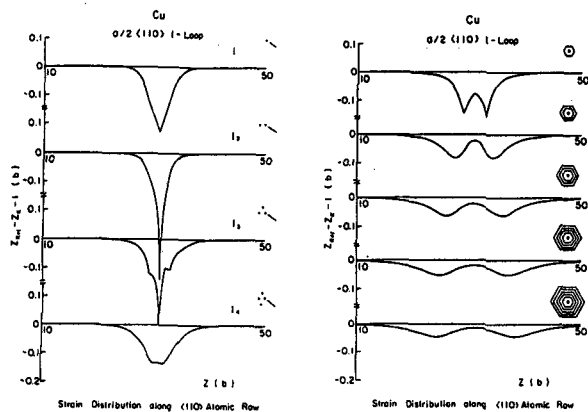


Fig. 5 Strain distribution on $\langle 110 \rangle$ atomic row on which a component crowdion of the I-loop is located for Cu (the atomic row is designated by an arrow or on the central position of the loop)

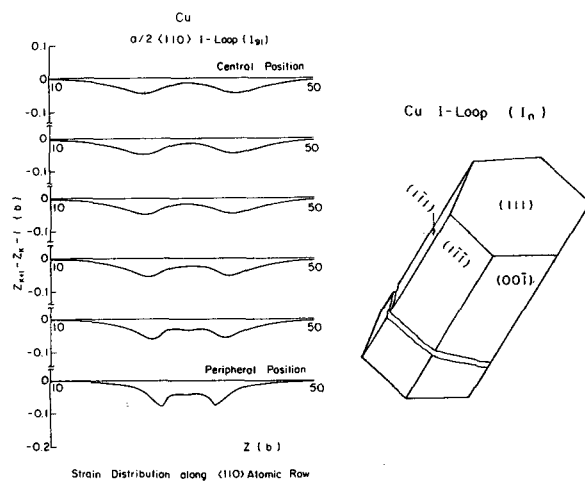


Fig. 6 Strain distribution as in Fig. 5 but in different atomic rows, especially at the peripheral position of the loop for Cu

3.2 Dislocation loops in Fe

Four kinds of the small interstitial loops, namely, i) $a/2\langle 111 \rangle\{110\}$ loop, ii) $a/2\langle 111 \rangle\{111\}$ loop, iii) $a\langle 100 \rangle\{100\}$ loop and iv) $a\langle 100 \rangle\{101\}$ loop were constructed in the model lattice. One example of the loop structure in Fe is shown in Fig. 7, where $a/2\langle 111 \rangle\{110\}$ loop consisting of 19 self interstitial atoms ($\langle 111 \rangle$ crowdions) is drawn through the top view and the side view. The formation energy and the

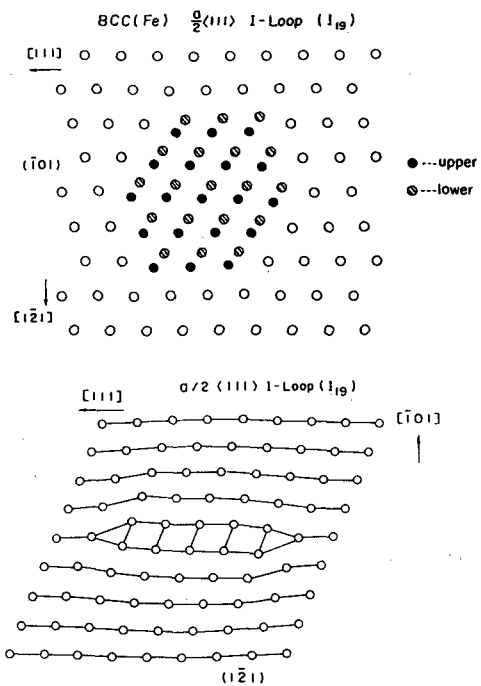


Fig. 7 Atomic structure of I-loop (I_{19}) in Fe
binding energy per one interstitial atom were calculated for each type of the dislocation loop as a function of the number of the component interstitial atoms and the binding energy for $a/2\langle 111 \rangle\{110\}$ loop is shown in Fig. 8. The formation energy decreased in the order of a $\langle 100 \rangle\{110\}$ loop, a $\langle 100 \rangle\{100\}$ loop, $a/2\langle 111 \rangle\{111\}$ loop and $a/2\langle 111 \rangle\{110\}$ loop.

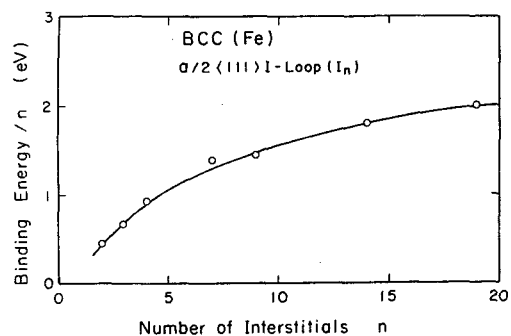


Fig. 8 Binding energy as a function of loop size in Fe
As in the case of Cu the strain distribution on the atomic row on which each component crowdion is located was obtained as a function of loop size and a position of the atomic row of the crowdion for the $a/2\langle 111 \rangle\{110\}$ loop and the result is shown in Fig.9. It is also found that in small interstitial clusters the

strain is localized as in the case of single crowdion, but in the larger clusters ($n > 10$) it is split into two parts. It is, however, well known that in Fe a dislocation is not split into two partial dislocations because of high stacking fault energy. Then the strain distribution on the atomic row on the peripheral position of the loop was also obtained, which shows non-split strain distribution as shown in Fig. 10 for the interstitial cluster of 91 crowdions. The strain distribution in the case of a straight edge dislocation in Fe was also obtained as a function of the distance from the slip plane and is shown in Fig. 11, where the strain has no tendency of split on the atomic row which is located just above the slip plane, but as the distance from the slip plane increases the split tendency appears as in the case of the dislocation loop. This suggests that the interstitial clusters tend to have the character of a dislocation as in the case of Cu.

It is recognized that during irradiation small interstitial loops are very mobile on one dimensional way and this is responsible for the production bias in the case of the irradiation where cascades of Frenkel pair production occur. As the simple shear stress cannot move a dislocation loop, the cylindrical shear was applied to the dislocation loop and the movement of the whole dislocation loop to one direction was observed as shown in Fig. 12.

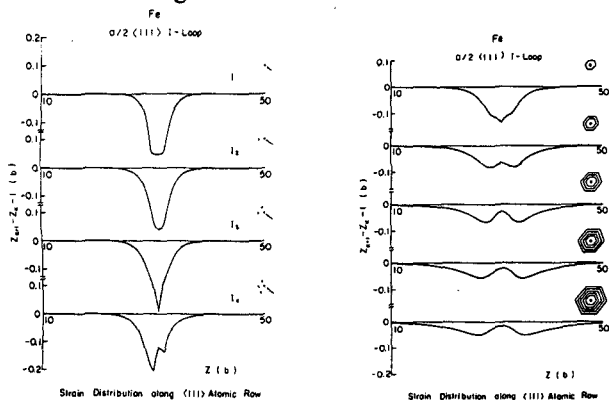


Fig. 9 Strain distribution on $\langle 111 \rangle$ atomic row for Fe

REFERENCES

1. C. H. Woo and B. N. Singh, *Phil. Mag. A*, 65 (1992) 889.

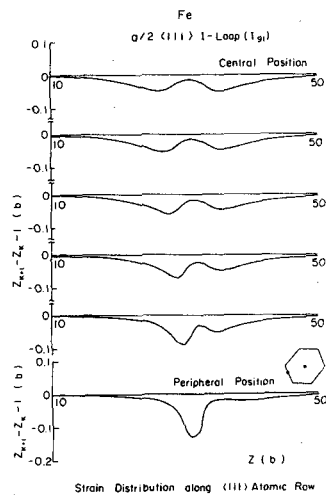


Fig. 10 Strain distribution (peripheral position (Fe))

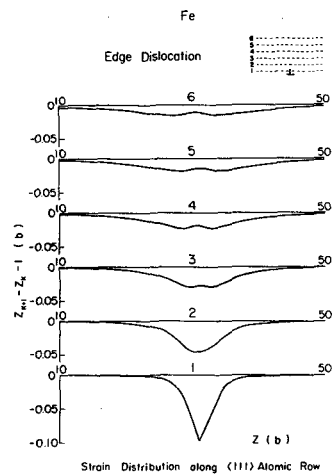


Fig. 11 Strain distribution (edge dislocation (Fe))

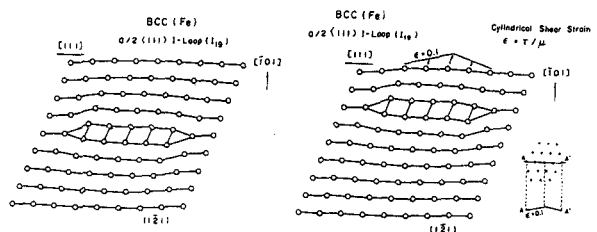


Fig. 12 Loop movement under cylindrical shear stress

2. H. L. Heinisch, B. N. Singh and T. Diaz de la Rubia, *J. Nucl. Mat.*, 212-215 (1994) 127.

3. G. I. Ackland, G. Tichy, V. Vitek and M. W. Finnis, *Phil. Mag. A*, 56 (1987) 735.

4. M. W. Finnis and J. E. Sinclair, *Phil. Mag. A*, 50 (1984) 45 and *Phil. Mag. A*, 53 (1986) 161 (erratum).